NeuroImage **14,** 486–500 (2001)
doi:10.1006/nimg.2001.0845, available online at http://www.idealibrary.com on IDEAL®

Spatial Normalization of Brain Images with Focal Lesions Using Cost Function Masking

Matthew Brett,*[,1] Alexander P. Leff,† Chris Rorden,‡ and John Ashburner§

**MRC Cognition and Brain Sciences Unit, 15 Chaucer Road, Cambridge CB2 2EF; †MRC Cyclotron Unit, Hammersmith Hospital, London; ‡University of Nottingham, Nottingham; and §Functional Imaging Laboratory, Institute of Neurology, London, United Kingdom*

Received May 30, 2000

In studies of patients with focal brain lesions, it is often useful to coregister an image of the patient's brain to that of another subject or a standard template. We refer to this process as spatial normalization. Spatial normalization can improve the presentation and analysis of lesion location in neuropsychological studies; it can also allow other data, for example from functional imaging, to be compared to data from other patients or normal controls. In functional imaging, the standard procedure for spatial normalization is to use an automated algorithm, which minimizes a measure of difference between image and template, based on image intensity values. These algorithms usually optimize both linear (translations, rotations, zooms, and shears) and nonlinear transforms. In the presence of a focal lesion, automated algorithms attempt to reduce image mismatch between template and image at the site of the lesion. This can lead to significant inappropriate image distortion, especially when nonlinear transforms are used. One solution is to use cost-function masking—masking the areas used in the calculation of image difference—to exclude the area of the lesion, so that the lesion does not bias the transformations. We introduce and evaluate this technique using normalizations of a selection of brains with focal lesions and normal brains with simulated lesions. Our results suggest that cost-function masking is superior to the standard approach to this problem, which is affine-only normalization; we propose that cost-function masking should be used routinely for normalizations of brains with focal lesions. © 2001 Academic Press

INTRODUCTION

Studies on patients with neurological disease often involve the analysis and display of brain images. These images may need to be spatially matched to a standard template, a process we will refer to as spatial normalization. In this paper we describe and evaluate a technique for spatial normalization of brains with focal lesions.

Spatial normalization can be useful to answer anatomical and physiological questions. For example, in studies of patients with focal brain lesions, it is common to represent the position and extent of the lesions in terms of a standard brain template. This allows the reader to more readily appreciate the site of the lesion in relation to those of other patients from the same or other series. If there is other information that has been registered to the same template, such as functional imaging data or estimated cytoarchitecture, then this can be related to the patient's lesion. Group studies in neuropsychology may be interested in the overlap of lesions for patients with a particular pattern of deficit, on the basis that, if the common deficit is due to damage of one brain area, this area will be contained within the overlap of the lesions. The overlap analysis requires that the location of the patients' lesions be transformed from the definition on the patient's own scan to an equivalent position on a template. Normalization to a template is also advantageous when there are neurophysiological data from a patient's brain that can be located spatially—for example, PET blood flow data or FMRI. The transformation may allow direct comparison with data from normal subjects, or with data from other patients.

Spatial normalization can be manual or automated. Early approaches used manual normalization, which involved painstaking estimation of lesion location from the patient's image (source image) on a set of standard brain slices (Mazzocchi and Vignolo, 1978; Damasio and Damasio, 1989). This required considerable input from a skilled operator. Talairach and Tournoux (1988) later suggested a transformation algorithm to a standard atlas involving the identification of various brain landmarks and piecemeal scaling of brain quadrants. As imaging software developed, programs became available that allowed the user to adjust spatial trans-

[1] To whom correspondence and reprint requests should be addressed. Fax: +44(0)1223 359062. E-mail: matthew.brett@mrc-cbu.cam.ac.uk.

1053-8119/01 $35.00

formations interactively to match two brain volumes (e.g., Evans *et al.*, 1991; Frank *et al.*, 1997). These and similar techniques suffer from being slow, operator dependent, and allowing only a restricted range of transforms to the image. However, they have the advantage that the transforms are robust to a wide variety of pathologies.

An alternative approach has been to use automated brain registration algorithms, such as AIR (Woods *et al.*, 1992), MNI_AutoReg/ANIMAL (Collins *et al.*, 1994), or SPM (Friston *et al.*, 1995). These algorithms use the differences in intensity values of the source image and the template to derive a mathematical measure of mismatch between the images—a "cost function." In SPM this cost function is the sum of the squared differences (χ^2) between the image voxel intensities. The automated algorithms use optimization methods to minimize image mismatch, by varying parameters for a given set of spatial transforms. The source and template image are usually smoothed before normalization, so that the algorithm matches the overall brain shape, rather than fine detail. The images are then aligned using linear (affine) transformations, which may be some or all of translations, rotations, zooms and shears. In a final step, the image to be matched is further transformed using nonlinear functions, such as discrete cosine transforms (SPM) or polynomials (AIR). The nonlinear transformations allow close matching of image detail, and would be difficult to determine manually, because they are complex for a human user to visualize. Thus one can calculate a match between the images with little or no operator intervention and which is reproducible between laboratories.

The template used for such normalizations is usually an image derived from an average of a number of MRI scans from neurologically healthy adults. For example, the default template for the most recent version of SPM (SPM99—http://www.fil.ion.ucl.ac.uk/spm) is an average of coregistered MRI brain scans from 152 healthy individuals; this template is a standard image provided by the Montreal Neurological Institute (MNI).

However, a problem arises if the brain to be normalized has an area of damage, or abnormal areas of large signal change, such as an aneurysm clip artefact. A lesion or artefact in the image will usually be of very different intensity from the equivalent area in the template. For this reason, even when the rest of the brain is well matched to the template, the cost function will be high in the area of the lesion. This is illustrated in Fig. 1.

Figure 1A shows an MRI scan from a patient with an area of low density in the left anterior frontal lobe caused by a stroke. For the sake of illustration, the image has already been roughly matched to the template, shown in Fig. 1B, using affine only normalization. The cost function in SPM is the squared difference between the (smoothed) images; Fig. 1C shows the image of this cost function. Voxels with high squared difference are shown as bright on the image. The area of lesion still contributes strongly to the cost function, even though the images are reasonably well matched. In such a case, the algorithm may estimate that further transformations are necessary in order to minimize the difference between the source and the template in the area of the lesion, at the expense of matching elsewhere in the image.

When estimating parameters for the linear transforms, any changes to the parameters that can minimize the differences between the lesion and the template are likely to cause widespread mismatches elsewhere. Thus, automated estimates of affine transforms are relatively robust to the effects of lesions; Fig. 1A shows the result of normalizing using affine parameters only, using SPM99. However, the lesion may have a strong influence on the parameters of the nonlinear transforms, which can have effects that are relatively local. The result is usually that the nonlinear warping reduces the size of the lesion. Figure 1D shows the image after performing affine normalization and nonlinear warping in SPM99. The nonlinear warping has crushed the lesion, causing marked distortion nearby.

Despite these pitfalls, it is common for authors using normalization of damaged brains not to specify their normalization method. Two exceptions are Fiez *et al.* (2000) and Weiller *et al.* (1995). Fiez *et al.* looked at normalizations of a set of 10 brain images with left frontal damage. They compared the normalization performance of their own manual warping technique to that of a modified version of the standard AIR algorithm. Using various measures of agreement on lesion volume and shape, they showed that the AIR normalizations, which used affine and nonlinear parameters, gave comparable results to those for manual warping by two observers. However, for two of the 10 images normalized, the results of the AIR technique differed markedly from those of the manual warping. It is also not clear to what extent the lesions may in fact have been excluded from the calculation of the normalization. AIR implicitly excludes voxels with low signal from the match; this is a type of lesion masking, which is the technique we evaluate in this paper. The images used by Fiez *et al.* are all likely to have had lesions of low signal intensity.

The other paper to describe their normalizations of damaged brains is Weiller *et al.* (1995). These authors normalized images from patients with left parietotemporal lesions, using an image for the normalization that was computed from the average of the original scan and its mirror image. This will reduce the abnormal signal due to the lesion on one side, at the expense of extending the potential distortions to both hemi-

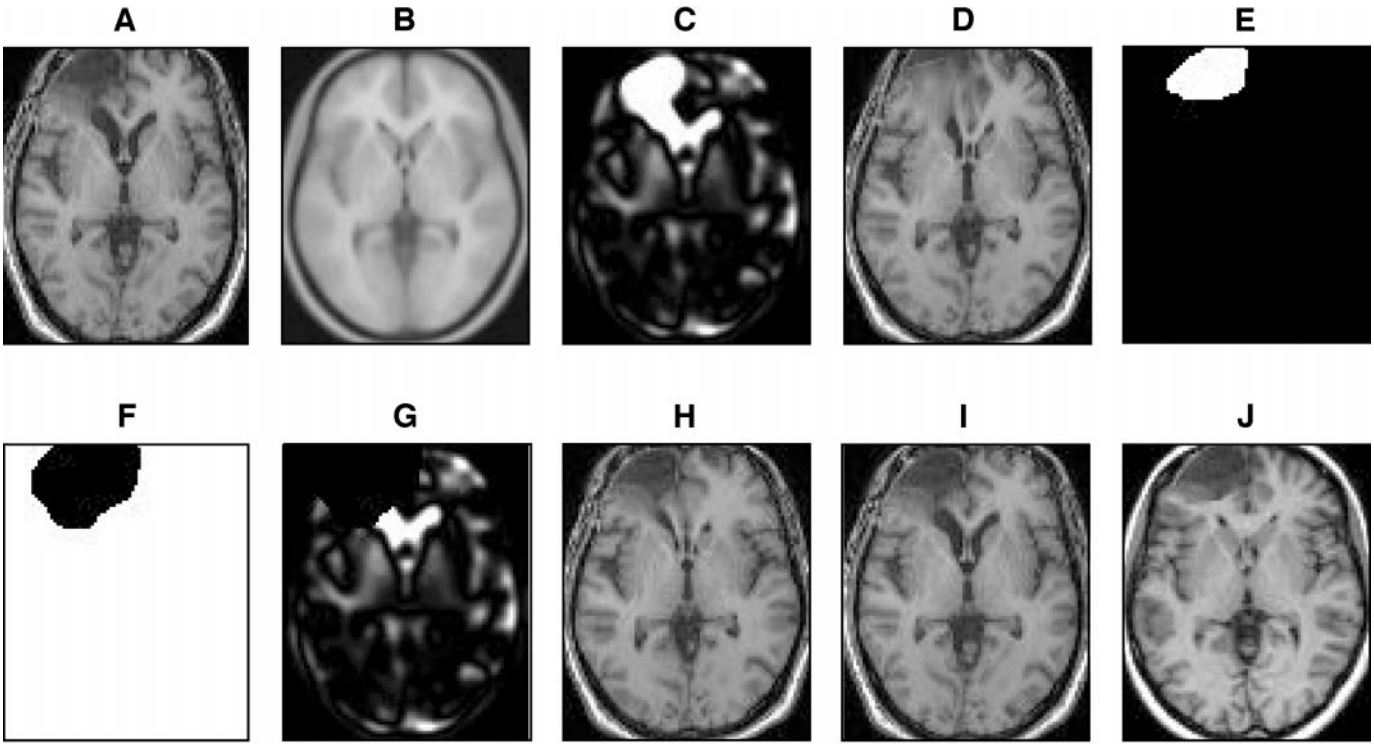

FIG. 1. Normalizations, cost functions, and masks for an example image. (A) Rough normalization of an image with frontal lobe lesion, using affine only normalization; (B) template; (C) image of squared difference between smoothed source image A and template B—mismatch for skull and scalp has been removed with a brain masking image (see Theory); (D) standard normalization of A with nonlinear functions—note marked image distortion; (E) lesion definition image; (F) resulting masking image; (G) cost function C with mask F applied; (H) normalization using affine and nonlinear functions with cost function masking; (I) affine only normalization with cost function masking; (J) simulated lesion in normal MRI.

spheres, and adding error to parts of the brain that are not symmetrical, such as the planum temporale. A series of recent papers have used spatial normalization in studies of aphasia with activation PET (Price *et al.*, 1998; Mummery *et al.*, 1999; Warburton *et al.*, 1999). Although these papers do not describe the normalization procedure, they did in fact use affine-only transformation (Richard Wise, personal communication). In other studies it is not clear what method has been used (Musso *et al.*, 1999; Specht *et al.*, 1999).

The affine-only approach is less sensitive to bias caused by lesions, but it is not ideal. While more robust than nonlinear normalization, it can still be influenced by the lesion. This can be seen by comparing Fig. 1A to the template in Fig. 1B. In the affine only normalization (Fig. 1A) the lesion has caused the normalization to stretch the front of the brain, and the lesion, so that it overlies low signal from the CSF and skull. The linear functions also provide a less accurate match of local brain detail than the affine and nonlinear combination (Ashburner and Friston, 1999).

A simple solution to this problem of template/lesion mismatch is to restrict the cost function to areas of brain outside the abnormality. In this way the calculated transforms are no longer biased by the effect of the lesion. This technique has been used previously for realignment and coregistration of images within individual subjects. The AIR program (Woods *et al.*, 1992) implicitly excludes voxels from the optimization that have signal below a given intensity threshold, on the basis that the voxels are likely to be outside the brain. This thresholding technique has been used more explicitly with AIR for removing less important voxels from calculation of realignment parameters in FMRI time series collected with surface coils (Hajnal *et al.*, 1994), and to remove lesioned areas from the calculation of matches between images of different modality from the same subjects (see section 12 in the methods of (West *et al.*, 1997)).

In this study, we have implemented cost function masking using a mask image, which has values of 1 outside the lesion and 0 within the lesion. The user first defines the area of the lesion (see Fig. 1E). The lesion definition is inverted and expanded, to take account of the effect of the smoothing of the source image before normalization (see Methods). Figure 1F shows such a masking image, and Fig. 1G shows the variance image (cost function) after the mask has been applied. Figure 1H shows the result of using this mask during an affine and nonlinear normalization. The image is

well matched to the template, without obvious distortion of the lesion. The goal of this paper is to investigate whether it is useful to use such a masking image to improve normalization of brains with areas of abnormality.

THEORY

The objective of spatial normalization is to estimate the most probable spatial transformation that matches a source image to a template image. The procedure described here is for the algorithms used in SPM99, although similar principles apply for other automated normalization methods. The goal of the affine and the nonlinear stages of the normalization is to find the optimum set of transforms that will minimize the cost function, which is the sum of the squared differences (χ^2), between the source and template voxel intensities. If we sample the template image at N voxels, and sample the source image at the equivalent voxel locations, we can obtain the difference in voxel intensity d_i for voxel i, where i indexes the voxel $1 \ldots N$. We wish to optimize a set of parameters for our spatial transforms; let us term the vector of these parameters $\mathbf{p}$. In the case of the affine transformations, $\mathbf{p}$ could be a vector of length 12, where the first three values are the transformations in mm in x, y, and z, values four to six are rotations around the x, y, and z axes, and so on. At each voxel there will be a function $d_i(\mathbf{p})$, of unknown shape, which is the difference between the source and template images at that voxel as a function of the parameters $\mathbf{p}$. In order to minimize this function, we can use an iterative algorithm (Press *et al.*, 1992). This proceeds by first calculating $d_i(\mathbf{p})$ for a starting estimate of $\mathbf{p}$. Then for each of the parameters, we calculate the rate of change of d_i for small changes of the parameter, i.e., we calculate $\partial d_i(\mathbf{p})/\partial p_1$, $\partial d_i(\mathbf{p})/\partial p_2 \ldots$. This information can be used to estimate the value of d_i for a given change in parameters $\mathbf{t}$, using the first order approximation of Taylor's theorem:

$$d_i(\mathbf{p} + \mathbf{t}) = d_i(\mathbf{p}) + t_1 \frac{\partial d_i(\mathbf{p})}{\partial p_1} + t_2 \frac{\partial d_i(\mathbf{p})}{\partial p_2} \cdots$$

Across voxels, this can be formulated as:

$$\begin{bmatrix} d_1(\mathbf{p}+\mathbf{t}) \\ d_2(\mathbf{p}+\mathbf{t}) \\ \vdots \end{bmatrix} = \begin{bmatrix} d_1(\mathbf{p}) \\ d_2(\mathbf{p}) \\ \vdots \end{bmatrix} + \begin{bmatrix} \frac{\partial d_1(\mathbf{p})}{\partial p_1} & \frac{\partial d_1(\mathbf{p})}{\partial p_2} & \cdots \\ \frac{\partial d_2(\mathbf{p})}{\partial p_1} & \frac{\partial d_2(\mathbf{p})}{\partial p_2} & \cdots \\ \vdots & \vdots & \ddots \end{bmatrix} \begin{bmatrix} t_1 \\ t_2 \\ \vdots \end{bmatrix},$$

which is minimized when:

$$\mathbf{A}\mathbf{t} \simeq \mathbf{b}, \tag{1}$$

where

$$\mathbf{A} = \begin{bmatrix} -\frac{\partial d_1(\mathbf{p})}{\partial p_1} & -\frac{\partial d_1(\mathbf{p})}{\partial p_2} & \cdots \\ -\frac{\partial d_2(\mathbf{p})}{\partial p_1} & -\frac{\partial d_2(\mathbf{p})}{\partial p_2} & \cdots \\ \vdots & \vdots & \ddots \end{bmatrix},$$

$$\mathbf{t} = \begin{bmatrix} t_1 \\ t_2 \\ \vdots \end{bmatrix} \text{ and } \mathbf{b} = \begin{bmatrix} d_1(\mathbf{p}) \\ d_2(\mathbf{p}) \\ \vdots \end{bmatrix}.$$

We can solve the equations above to give the parameter changes $\mathbf{t}$ that minimize the sum of the squared image differences across voxels:

$$\mathbf{t} = (\mathbf{A}^T\mathbf{A})^{-1}\mathbf{A}^T\mathbf{b}. \tag{2}$$

This estimate of $\mathbf{t}$ allows an iterative scheme; for any iteration n, the parameters $\mathbf{p}$ are updated so that $\mathbf{p}^{(n+1)} = \mathbf{p}^{(n)} + \mathbf{t}$. The iterations proceed until the sum of squared difference is minimized. In the case of the affine step, the parameters $\mathbf{p}$ to be optimized are the translations, rotations, zooms, and shears of the source image relative to the template. For the nonlinear step, the parameters are coefficients for a series of discrete cosine transform basis functions (Ashburner and Friston, 1999).

There are several important additions to the algorithm above, which are used by default in SPM99. First, before normalization, the source and template images are smoothed with an 8-mm isotropic Gaussian filter to decrease the chance that the optimization will be caught in a local minimum. Second, SPM99 weights the optimization for both affine and nonlinear steps using a Bayesian approach. In the case of the affine transforms, Bayesian priors for the distributions of zooms and shears are derived from the results of 51 successful normalizations using the standard least squares algorithm described above (Ashburner *et al.*, 1997). For the nonlinear step, the algorithm simultaneously minimizes both the sum of squared difference between the images and the membrane energy of the deformation field (Ashburner and Friston, 1999). The membrane energy is a measure of the smoothness of the deformation, where low values for membrane en-

ergy represent smoother deformations. By attempting to minimize the membrane energy, the algorithm biases the deformations to be smooth. Last, SPM99 uses a masking image in the same space as the template that sets the cost function to zero in areas outside the template brain, so that the algorithm does not attempt to optimize transformation parameters that will reduce mismatches of scalp and skull between the source and template. We will describe the use of this template cost-function masking image in more detail below.

The bias we see when normalizing brains with lesions is due to the tendency of template/lesion mismatch to drive the optimization to produce inappropriate transformations. To remove this bias, we can mask the cost function so that the mismatch in the area of the lesion no longer contributes to the parameter optimization. The masking is implemented using an image, in the same space as the source image, which contains voxel values from 0 to 1, expressing the weight to be given to the cost function in that voxel in the optimization. Thus, if w_i is the voxel value from the masking image at voxel i, then the design matrix **A** in the optimization from Eq. (2) becomes:

$$\mathbf{A} = \begin{bmatrix} -\dfrac{\partial d_1(\mathbf{p})}{\partial p_1} w_1 & -\dfrac{\partial d_1(\mathbf{p})}{\partial p_2} w_1 & \cdots \\ -\dfrac{\partial d_2(\mathbf{p})}{\partial p_1} w_2 & -\dfrac{\partial d_2(\mathbf{p})}{\partial p_2} w_2 & \cdots \\ \vdots & \vdots & \ddots \end{bmatrix}. \qquad (3)$$

In the simplest case, the masking image will be binary, containing 1 in voxels corresponding to normal brain and 0 in the voxels corresponding to the lesion. One can see from Eqs. (1) and (3) that changes in image gradients $\partial d_i(\mathbf{p})/\partial p_1$, $\partial d_i(\mathbf{p})/\partial p_2 \ldots$, and the cost function d_i, for voxels where $w_i = 0$ will have no influence on the parameters **t**. The mask therefore has the effect of setting to zero the cost function in the lesioned area, so that the lesion no longer influences the optimization. Figures 1F and 1H show a mask image and the resulting normalization.

In fact, SPM assumes the use of a binary cost function mask for the source image; this is because, for a continuous source masking image, the equations above would also require a term for the gradient of the source masking image. In practice, including such a term using discrete (voxel by voxel) gradient estimation leads to unstable solutions to the optimization. By using a binary mask we can assume that the source masking image has zero gradient at each sample point, and therefore remove the gradient term.

We mentioned above that SPM99 is also able to use cost function masking for the template image, to restrict the optimization to voxels within the brain (Ashburner *et al.*, 1998). Here the values of w_i are from an image in same voxel space as the template, and $w_i = 0$ for voxels outside the brain—e.g., corresponding to scalp or skull. Unlike the source weighting image, this image can be continuous, containing values between 0 and 1. In fact this is the case for the default template masking image, which is the `brainmask.img` in the SPM `apriori` directory. This image is based on an image that contained ones and zeros, where ones represent voxels that are within the brain in the MNI average brain template. To create `brainmask.img`, the original image has been smoothed using an 8-mm FWHM Gaussian. Thus the voxel values reflect the proportion of the signal in the matching voxel of the smoothed template that has been derived from structures within the brain. When the source and the template weighting images are used, the value for w_i used in A [Eq. (3)] is given by the harmonic mean of w_i^s and w_i^t, where w_i^s is the weight for voxel i from the source masking image, and w_i^t is the weight from the template masking image.

METHOD

The evaluations that follow are designed to address three main issues. First, cost-function masking requires that the user define the position and extent of the abnormal signal within the source image. We want to know the extent to which the normalization is affected by the differences in the masks defined by different observers. Second, the source image will be smoothed before normalization, so that the abnormal signal will affect a larger volume in the image. We define how far the cost function mask must be extended to allow for this smoothing. Finally, we compare the cost function masking technique to the *de facto* standard, which is affine-only normalization.

A problem for all these evaluations is that there is no accepted standard measure for the success of a normalization. We have approached this problem in two ways. In the latter part of this section, we have used some simple summary images of the normalizations to give a qualitative impression of the performance of the different methods. In the first part of this section, we looked at normalizations of normal brain scans with simulated lesions. In this way, we can compare a normalization of a scan with a simulated lesion, to a useful standard, which is the default normalization of the same brain without a lesion.

All the evaluations make use of 10 TI MRI images of brains with a variety of lesions. Figure 2 shows representative axial slices from the 10 images. We selected the images from those available to us to provide a wide range of pathology, including images or artefacts with high and low signal intensity. An image was accepted if the scan was of reasonable quality and the lesion was relatively confined and unilateral.

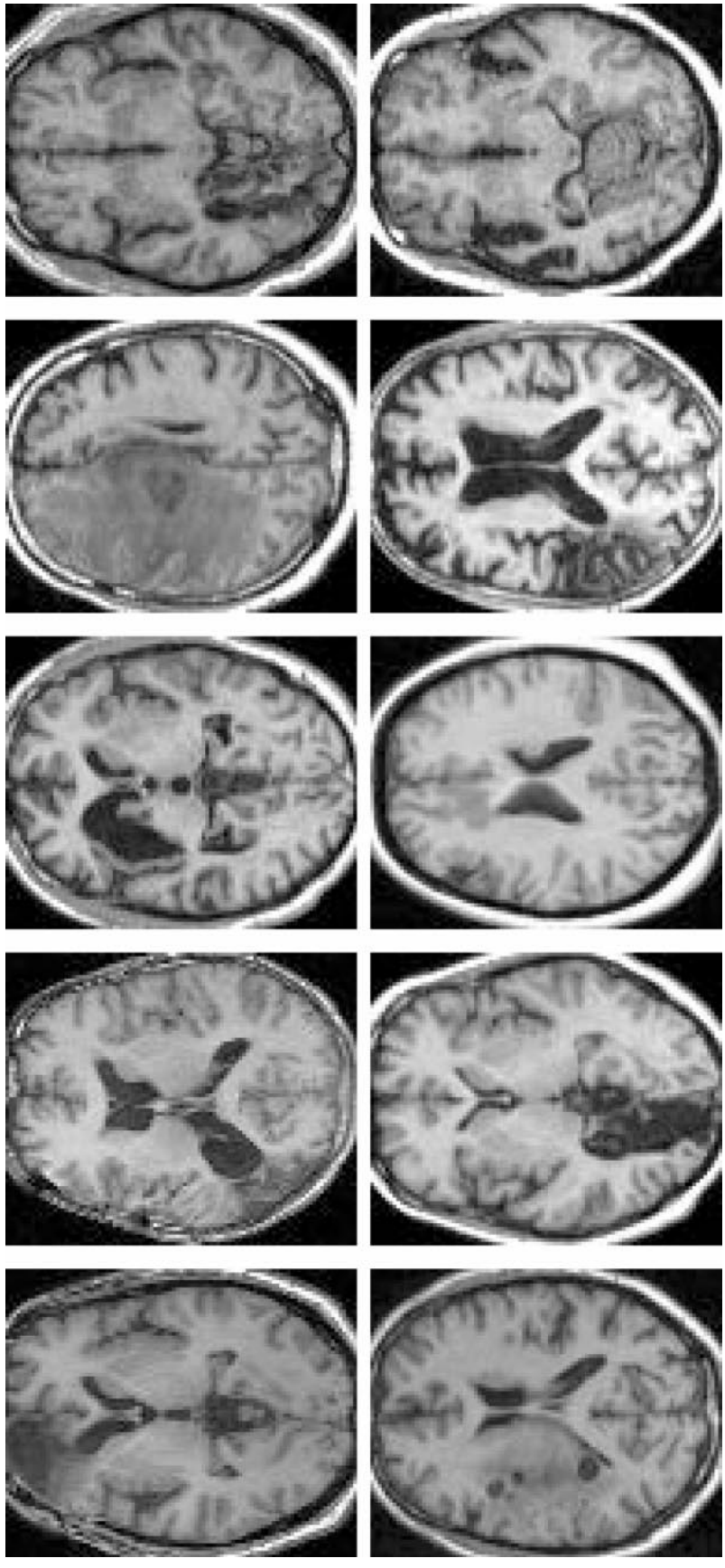

FIG. 2. Brain images used in the validation. Starting from top left going clockwise, the abnormalities are: left anterior frontal infarct (image A from Fig. 1); left anterior communicating artery aneurysm, with clip artefact (not shown) and temporoparietal infarct; infarct in the left putamen/insula; metastasis above the corpus callosum with extensive oedema, left occipitotemporal infarct; marked temporal lobe atrophy left greater than right; left temporoparietal infarct; multiple areas of cortical dysplasia; left occipitotemporal infarct, left frontoparietal loculated infarct. For ease of display, the images have been normalized using affine parameters only and cost function masking.

For the cost function masking, we created four sets of lesion definition images. Four observers independently defined the areas of abnormality on the 10 source images, to give four sets of lesion definitions, 1 . . . 4. The observers were instructed to draw as exactly as possible round the areas of abnormal signal within the brain. Enlarged ventricles were omitted from the lesion definition, but artefacts with abnormal signal such as aneurysm clip artefacts were included. Three observers had neurology training to residency level, and one was a psychologist experienced in the analysis of brain lesions. Lesion definition set 1 was defined using the image edit facility in Analyze AVW software (Mayo Biomedical Imaging Resource, Mayo Clinic, MN). The remaining sets were defined using MRIcro, a brain image display utility (http://www.psychology.nottingham.ac.uk/staff/cr1/mricro.html). The lesion definitions resulted in images that had the value of 1 for voxels inside the abnormal areas and 0 elsewhere. An example slice from such an image is shown in Fig. 1E.

For all of the normalizations in the following section we have used the default settings for SPM99 unless otherwise stated. With these settings the program uses a template mask to exclude areas outside the brain from the cost function (see above). For the nonlinear normalizations we used medium regularization (the weight given to the term biasing the nonlinear transformations to be smooth—see Theory). We used 7 × 8 × 7 discrete cosine transform basis functions and 12 iterations of nonlinear optimization. The template we used was the default `T1.img`, in the SPM templates directory, which is the MNI 152 average brain, presmoothed to 8 mm for use in normalization (see http://www.mrc-cbu.cam.ac.uk/Imaging/templates.html). Before all normalizations we used the SPM display utility to set the orientation of the source to a rough match with the template, in terms of translations and rotations. All image resampling used trilinear interpolation. Resampled binary images were rebinarized by rounding to voxel values of 0 or 1. For several steps in the processing, we needed to define which voxels were within the brain; for this we used a thresholded template brain mask (TTBM). This was simply the `brainmask.img` described above, thresholded so that values above 0.5 were set to 1 and elsewhere to 0. As expected, this image corresponded closely to the brain outline of the template.

The simulated lesion images were created by reslicing the lesions from the damaged brains into normal brain images. We first took 10 T1-weighted MRI scans of brains with no neurological abnormality, and arbitrarily paired each image with one of the lesioned brains, to create 10 normal–abnormal pairs. For each pair, we used the SPM affine only normalization to calculate the parameters needed to match the normal and the lesioned image to the MNI template. The affine normalizations of the abnormal brains gave acceptable results for all 10 brains; the least satisfactory is shown in Fig. 1A. Using the combined parameters of the two normalizations, we resliced the abnormal image into the voxel space of the untransformed normal brain. The same parameters were used to reslice the matching lesion definition image from mask set 1 into the voxel space of the normal brain. Using the normalization of the normal brain, we also resliced the TTBM into the same voxel space. In order to match the intensity of the resliced abnormal image to the normal image, we derived a scale factor s, for the resliced abnormal image. The scale factor makes use of a masked mean value for the normal and resliced abnormal images.

The masked mean is simply the mean intensity value of an image, for voxels inside the brain, but outside the area of a lesion. Let us say that we have an image, **x**, a lesion definition, **ld**, and a brain mask **bm**, all in the same voxel space. **ld** has ones in voxels corresponding to the lesion in **x**, and zeros elsewhere; **bm** has ones in voxels corresponding to the brain volume in **x**, and zeros elsewhere. The masked mean for **x** is the mean of all voxels in **x**, for which both of the following are true: (1) the corresponding voxel in **ld** contains zero (voxel is outside the lesion), and (2) the corresponding voxel in **bm** contains a one (voxel is within the brain).

Here, the scale factor s for the resliced abnormal image is given by the masked mean of the normal image, divided by the masked mean for the resliced abnormal image, where the lesion definition for both is the resliced lesion definition, and the brain mask is the resliced TTBM.

We then created a new image **sl**, with a simulated lesion, by inserting the lesion of the resliced abnormal image into the original normal image, prior to normalization. If sl_i is the value of image **sl** at voxel i, **rld** is the resliced lesion definition image, and n_i, rld_i, and ra_i are the values of the matching voxel in **n**, **rld**, and **ra**, respectively, then

$$sl_i = \begin{cases} ra_i \cdot s & \text{if } rld_i = 1 \\ n_i & \text{otherwise.} \end{cases}$$

We repeated this process for each normal/abnormal image pair. An example of an image with a simulated lesion is shown in Fig. 1J. For display, the image in the figure has been resliced to the space of the template using the affine normalization parameters for the paired normal image, before the lesion was inserted.

For each normal/abnormal pair, we then resliced the lesion definitions from sets 2 to 4, to the voxel space of the new simulated lesion image, using the original affine normalizations for the normal and abnormal scans.

We can now compare normalizations of the brains with simulated lesions to the standard normalization of the same brain without the lesion. Normalizations can be compared using deformation fields. These are images, for each normalization, of the same voxel dimensions of the template image. The images contain, for each voxel, the displacement that the normalization has estimated in order to reach the position of the matching voxel in the source image. The displacements are translations, in millimeters, in the *X*, *Y*, and *Z* direction, which can be simply calculated from the normalization parameters. When two normalizations are similar, then the voxel displacements will be similar, reflecting that fact that the voxel values for the normalized image will have been obtained from similar points in the source image, across normalizations. The distance $d_i^{a,b}$ between the displacements at a single voxel *i*, for two normalizations *a* and *b*, is given by:

$$d_i^{a,b} = \sqrt{(x_i^a - x_i^b)^2 + (y_i^a - y_i^b)^2 + (z_i^a - z_i^b)^2},$$

where x_i^a is the translation in *X* for voxel *i* in the deformation field for normalization *a*. A measure of the overall similarity between two normalizations *a* and *b* is the root mean square (RMS) displacement of one deformation field relative to the other:

$$RMS_{a,b} = \sqrt{\sum_{i=1}^{N} (d_i^{a,b})^2 / N},$$

where *i* indexes the voxels within the brain 1 . . . *N*. Voxels were deemed to be within the brain when the matching voxel in the TTBM had a value of 1.

We were interested to determine the optimum distance to expand the area defined by the lesion definitions to allow for the smoothing of the source image during normalization. We therefore took each of the lesion definitions from sets 2 . . . 4, and smoothed them using a Gaussian filter of FWHM of 8 mm. We then inverted and thresholded the resulting images at a variety of thresholds, to create *processed normalization masks*. If pnm_i is the value of the new processed lesion mask at voxel *i*, sld_i is the equivalent value for the smoothed lesion definition image, and *t* is the threshold, then:

$$pnm_i = \begin{cases} 1 & \text{if } sld_i <= t \\ 0 & \text{otherwise} \end{cases}. \qquad (4)$$

The voxel values in the smoothed lesion definition can be thought of as the proportion of the signal at that voxel, after smoothing, that has been derived from voxels within the lesion. *t* is therefore the maximum proportion of signal from within the lesion that will allow that voxel to be retained in the normalization. *t* can be expressed as a percentage, so that a *t* of 0.25 corresponds to a threshold of 25%.

Each of the 10 resliced lesion definitions from sets 2 . . . 4 were processed in this way, using thresholds of 25, 10, 5, 1, 0.1, 0.001, and 0.0001%. These thresholds result in an expansion of the masked area beyond the area of the lesion definition; the thresholds above correspond to expansions of 2.3, 4.3, 5.5, 7.7, 9.6, 10.1, and 10.2 mm, respectively. The expansion for the 0.1% threshold is shown by comparing the lesion definition in Fig. 1E to the resulting processed mask in Fig. 1F.

We normalized the 10 images with simulated lesions, using affine plus nonlinear parameters and cost function masking. The masks were the processed normalization masks from the three resliced lesion definition sets 2 . . . 4, at the thresholds above, giving 3 × 7 sets of normalizations for each of the 10 images. We did not use lesion definition set 1 because it had been used to create the lesions. For comparison, we also normalized the same images without cost function masking, once using affine parameters only, and once using affine plus nonlinear parameters. Each individual normalization can be compared to the standard of the normalization of the same image, without the lesion, with both affine and nonlinear parameters. This gives an RMS value, in mm, for each candidate normalization of the images with simulated lesions. These values are displayed in Fig. 3.

The second part of our evaluation was to provide a qualitative assessment of normalizations of the original 10 images of damaged brains. Again, we want to compare the performance of affine only normalization to that of affine plus nonlinear normalization with cost function masking. We first normalized the 10 damaged brains, using masks based on lesion definition sets 1 . . . 4. To create processed normalization masks from the lesion definition image, we used the procedure above, which was smoothing of 8-mm FWHM, followed by thresholding, according to Eq. (4). For reasons discussed in the results section, we used a threshold of 0.1% to create the masks. We then normalized the 10 images with cost function masking, using each of the processed normalization images from lesion definitions 1 . . . 4, giving four normalizations for each image. We also normalized the 10 images using affine parameters only with no cost function masking. For each normalization, we resliced the abnormal image and the corresponding lesion definition image, using the normalization parameters, to give spatially normalized versions of both images. For the affine only normalization, which had no corresponding lesion definition, we resliced the images from lesion definition set 1.

To the extent that the normalizations have been successful, we would expect the normalized images to be similar to each other, and to the template image. To assess the similarity of the normalized images to each

other, we calculated a mean of the normalized images, for each of the five sets of normalizations. The mean image contained at every voxel the mean voxel intensity of the 10 images at that voxel. In order to calculate the mean, we divided the voxel values of each normalized image by a scale factor, to allow for differences in global intensity across images. If j indexes the normalized images 1 . . . 10, then the scale factor for image j, s_j, was the masked mean (see the Methods section) of $\mathbf{na_j}$, the normalized lesioned image. The lesion definition for the masked mean was the normalized lesion definition, for the matching lesion and lesion definition set, and the brain mask was simply the TTBM image.

In creating the mean, we are not expecting that areas of abnormality will be similar from one image to another. Therefore, voxel values were not used in the mean calculation if they fell within the abnormal area, as defined by the presence of a one in the normalized lesion definition image for that scan. If there were less than 6 scans for which there was a usable voxel value, then that voxel was set to zero in the mean image. Note that, after normalization, all the images are in the same voxel space, so that voxel i in one normalized image corresponds to voxel i in any other normalized image. Thus, let y_{ij} be the value from voxel i and normalized lesioned image j, and nld_{ij} be the value from the normalized lesion definition image from the same voxel. Then let

$$y_{ij}^{m} = \begin{cases} y_{ij}/s_j & \text{if } nld_{ij} = 0 \\ 0 & \text{otherwise} \end{cases},$$

and n_i^m be the number of scans for voxel i, where $nld_{ij} = 0$. Then the value for the mean image at voxel i is given by

$$mn_i = \begin{cases} \sum_{j=1}^{10} y_{ij}^{m}/n_i^m & \text{if } n_i^m > 5 \\ 0 & \text{otherwise} \end{cases}.$$

To assess the similarity of the images to the template, we have calculated template variance images. We first rescaled the intensity of the normalized images using the scalefactors described above. We also rescaled the template with a scalefactor, s_t, which was the mean of all voxels in the template within the brain, as indicated by a value of one in the matching voxel of the TTBM. We then subtracted the rescaled template image from each of the rescaled normalized images, and combined these difference images to create the template variance image. This image contained, at every voxel, the mean squared difference of intensity of the 10 normalized images from the template image. Again, we excluded voxels within the area of abnormality and set to zero voxels with fewer than 6 valid observations. Thus, if t_i is the value of voxel i in the template image, then the template/normalized image difference for scan j at voxel i is given by:

$$d_{ij}^{m} = \begin{cases} y_{ij}/s_j - t_i/s_t & \text{if } nld_{ij} = 0 \\ 0 & \text{otherwise} \end{cases},$$

and the value for the variance image $\mathbf{v}$, for voxel i, is given by:

$$v_i = \begin{cases} \sum_{j=1}^{10} (d_{ij}^{m})^2/(n_i^m - 1) & \text{if } n_i^m > 5 \\ 0 & \text{otherwise} \end{cases}.$$

The resulting image is a map of the variance of the 10 images from the template. Each of the lesion definition sets 1 . . . 4 gave a mean and variance image, as did the affine only normalization, giving a total of five mean/variance pairs.

RESULTS

Figure 3 shows results of the root mean squared (RMS) values for the normalizations of the simulated lesions.

Each RMS value compares the given normalization to the affine and nonlinear default normalization for the same brain, without the simulated lesion. Each of the 10 brains with simulated lesions is shown with a different symbol; thus all the points marked with an "*x*" refer to the simulated lesion image shown in Fig. 1J. The first two columns show the RMS values for the affine only and affine plus nonlinear normalizations, without any cost function masking. The values are relatively high, compared to the masked normalization values, shown in the rest of the plot. There is also considerable spread of the values across images, reflecting a high variability of normalization performance across images/lesions. The elevated RMS values for the unmasked affine matches reflects a combination of bias caused by the lesion, and the inability of the affine parameters to reproduce the distortions calculated for the nonlinear step in the normalizations of the unlesioned images. The unmasked nonlinear normalizations can reproduce some of the nonlinear distortions of the original normalizations and hence have reduced RMS values compared to the affine, but this is at the expense of allowing strong distortions in and around the lesions, reflected in the wide variation in the values across the 10 images.

The remaining columns in Fig. 3 give RMS values for masked normalizations using different mask thresholds [see Eq. (4)], and therefore mask expansions. For each threshold, there are three columns of RMS values, which are for normalizations using mask definitions

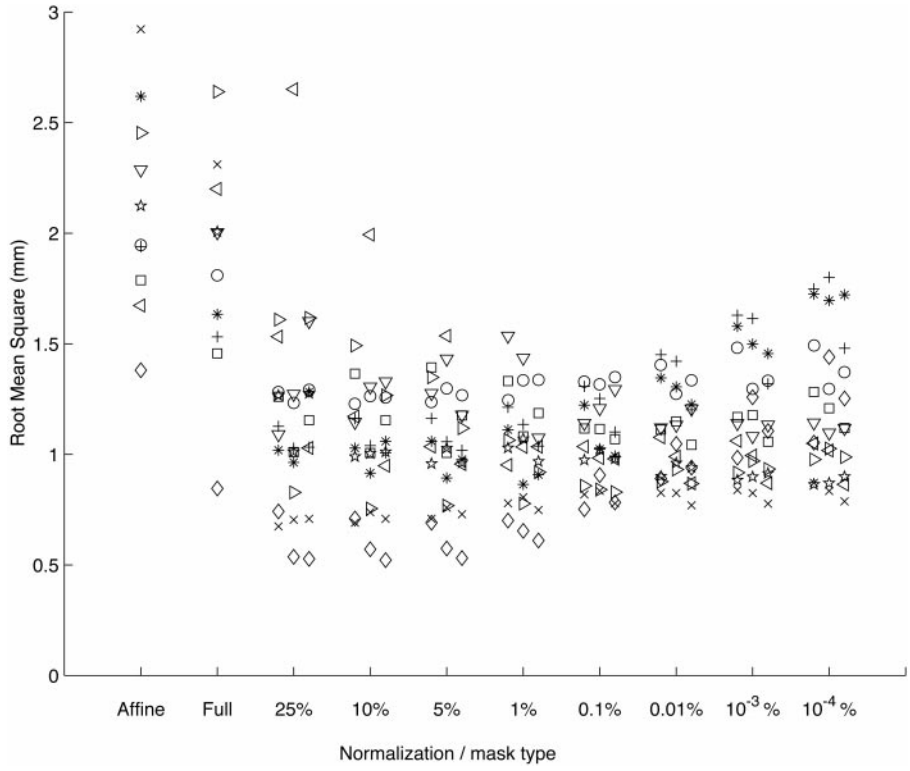

FIG. 3. Root mean square (RMS) values comparing normalizations of images with simulated lesions to matched normalizations of unlesioned brains. Each symbol represents normalizations for one simulated lesion image. The first and second columns show RMS values for normalizations without cost function masking, for affine only, and affine plus nonlinear normalizations. Subsequent columns show RMS values for affine plus nonlinear normalizations with cost function masking using different percentage thresholds for mask expansion relative to the lesion definition [see Eq. (4)]. The three columns for each threshold are for normalizations using masks from lesion definitions 2, 3, and 4.

from lesion definition sets 2 . . . 4. The figure therefore shows variability in normalization performance across images, and across observers defining the lesion. The ideal normalization method would provide low overall RMS values, with a narrow spread of values across images and with minimum variation between masks from different observers. On these three criteria, the mask threshold of 0.1% performs well, with a tight distribution of values across images, and very consistent performance across the three observers. With more liberal mask thresholds, more normal brain will be included in the normalization, as well as more signal from the edge of the lesion. This causes a marked increase in variability of normalization performance across images and observers. Conversely, with mask thresholds giving more expansion, the mask is excluding more normal brain, and thus the match becomes less constrained, and less similar to that for a normal brain, for which the whole brain is included. Therefore, to minimize variability across observers and images, as well as normalization bias caused by the lesion, we have adopted the conservative mask threshold of 0.1% for all subsequent processing.

Figure 1 shows the results of the different normalizations on an individual brain. The images in Fig. 1A and 1I both show the brain after affine only normalizations. Figure 1I was a normalization with cost function masking, and Fig. 1A was a normalization without cost function masking. For Fig. 1I, the overall shape is well matched to that of the template; the CSF spaces are wider in the damaged brain, in particular the left lateral ventricle next to the lesion. The image in Fig. 1A, affine only without cost function masking, is less well matched to the template. For this image, the lesion has caused a bias in the zoom in Y (anterior–posterior), so that the brain is longer than the template, and the anterior edge of the lesion overlies matching dark CSF space in the template. This obvious distortion using unmasked affine matching only occurred in this brain, and not in the other nine brains thus normalized. This is likely to be due to the width of the lesion, its very low intensity, and its site at the frontal pole. Figure 1H shows the image normalized with affine and nonlinear parameters and cost function masking. The brain edges are well matched to the template, and the nonlinear basis functions have transformed the image to reduce the size of the ventricles to better match those of the template.

Figure 4 shows the image of the mean voxel values across the normalized images of the 10 abnormal

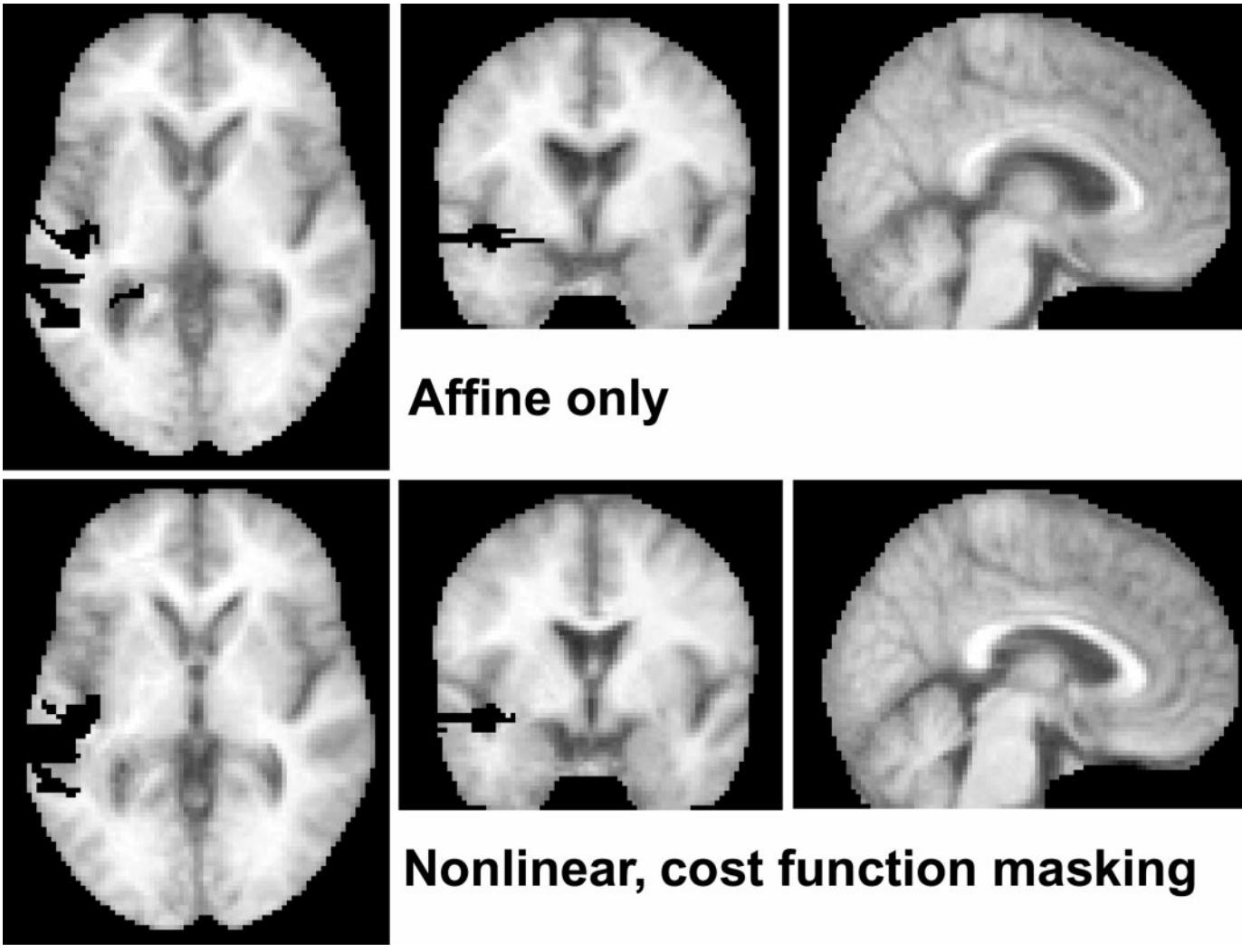

FIG. 4. Images of mean of rescaled normalized images from Fig. 2. Top panel: mean of images normalized using affine functions only; lower panel: mean of images normalized using affine and nonlinear functions and cost function masking. The cost function masks were derived from lesion definition set 1.

brains; these are the normalizations of the brains with real rather than simulated lesions.

The top three pictures are the sections from the affine only mean, and the bottom images show the mean of the nonlinear masked normalizations. For Fig. 4, and for Fig. 5, the images representing cost function masking are for normalizations using masks from lesion definition set 1. The mean and variance images for the other lesion sets were very similar to those for lesion set 1. This may not be surprising given the close agreement of the RMS scores for the different lesion sets using the 0.1% threshold mask. Note that the concentration of the lesions in our series in the left hemisphere has caused a degree of overlap of the lesion sites; the black area on the left of the image contains voxels where the voxel was outside the lesioned area in fewer than 6 of the 10 scans in the series.

The masked nonlinear mean has better contrast, especially around the borders of the ventricles. This higher contrast reflects less variability between images after normalization. On the affine image, there is a dark ring around the ventricles in the coronal slice, because white and gray matter near the ventricles is being averaged with CSF signal. This is because many of the images to normalize have enlarged ventricles relative to the template (see Fig. 2). The enlarged ventricles cannot be well matched with linear parameters whereas the local distortions available with nonlinear parameters are capable of such matching (see also Fig. 1). The corpus callosum is more clearly defined in the masked nonlinear mean, as is the upper brainstem, and to a lesser extent the cerebellum and lower occipital lobe (see the sagittal sections).

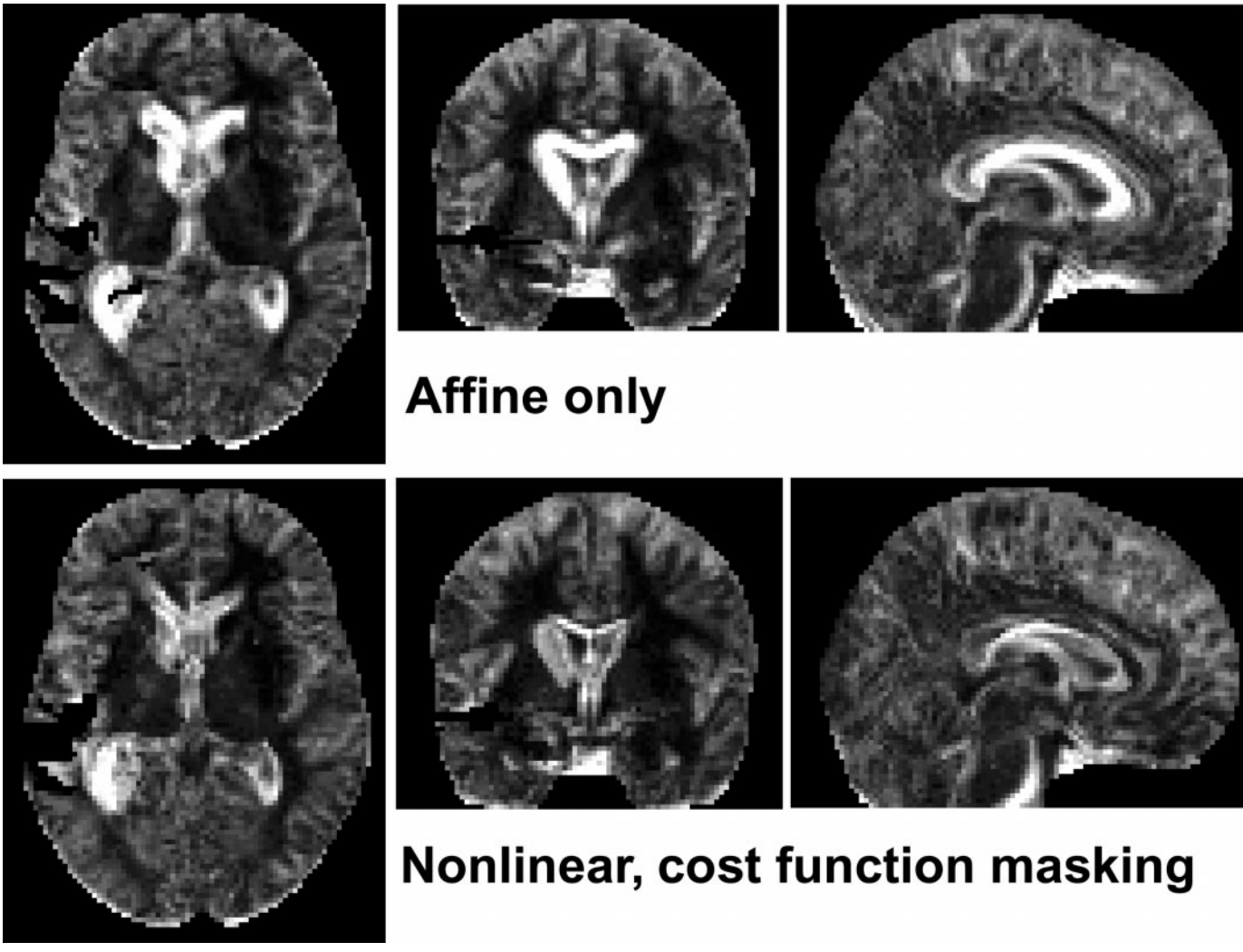

FIG. 5. Images of variance of normalized images from the template. Upper panel: variance of affine only normalized images; lower panel: variance of images normalized using affine and nonlinear functions with cost function masking, with masks from lesion set 1. Gray-scale to intensity mapping is the same for the upper and lower panel.

Figure 5 shows the image of the variance of the normalized images from the template.

Brighter voxel values therefore show areas where the normalized images have a high average difference in signal intensity from the template. The axial image (left) again emphasizes that the affine normalization has not been able to align CSF boundaries to those of the template. The axial images show that there is a large region of high variance around the frontal horns of the lateral ventricles which is less marked in the masked nonlinear than the affine variance image. In the coronal slices, there is apparent poor matching of the corpus callosum and the surrounding CSF, which again is more marked in the affine image. The left posterior horn of the lateral ventricle has an area of high variance surrounding it; this reflects the fact that most of the lesions in our series were on the left, and the lateral ventricle has become enlarged around the lesion site. The cost function masks around the lesions, once expanded for the normalization, have masked the expanded ventricle from compression during the nonlinear normalization. However, the normalized lesion definition, which has been used to remove damaged areas from the mean and variance calculation, is smaller than the mask used for normalization (see above and Fig. 1). Therefore, the smaller mask has exposed an area around the lesion that was not normalized using the nonlinear procedures, which may explain why the variance here is high for the masked nonlinear as well as the affine normalizations.

DISCUSSION

The problem that this paper has addressed is the tendency for automated warping algorithms to produce inappropriate solutions for brains with focal lesions.

More generally, these problems occur when matching brains to a template, where the brains to be matched have areas of signal, which do not have a corresponding area in the template. The solution we propose is to remove the area of abnormality from the calculation of the cost function, so that the optimization does not try to minimize differences between the source and template in the area of the lesion. Note that masking the abnormal region does not mean that areas under the mask remain untransformed, rather, a continuation of the solution for the unmasked portions of the image is applied to the area under the mask. This continuation will be constrained to be smooth by the use of the "nonlinear regularization" term in the normalization.

To evaluate this technique, we have compared the results of normalizing brains with real and simulated focal lesions, using affine only and masked nonlinear matching. Most previous studies that have used automated normalization for brains with lesions have used affine-only transformations (Price *et al.,* 1998; Mummery *et al.,* 1999; Warburton *et al.,* 1999). Our results suggest that normalization using cost function masking is superior to affine-only normalization for two related reasons. First, cost function masking can improve affine normalization in the presence of a lesion. Because of the bias caused by the lesion, even affine normalization can fail in certain situations, as shown by Fig. 1A. The influence of the lesion on the normalization parameters is difficult to quantify, depending on the size, location and signal of the lesion, and the quality of the match between source and template in other brain areas. Cost function masking removes the bias and should therefore be less susceptible to error than the affine-only method.

The second major advantage of cost function masking is that, using masking, we are able to use nonlinear deformations, without causing severe distortions in the lesioned image. Nonlinear deformations can greatly improve the quality of the normalization, both for normal brains (Ashburner and Friston, 1999), and for the brains in our sample. Although the affine transforms usually provide an acceptable match of the brain outline, they cannot match local brain detail, without disturbing alignment elsewhere. This is particularly obvious in our sample, because the brains of our patients have enlarged ventricles and sulci compared to those of the young normal brains used in the creation of the MNI template. Nonlinear normalization is able to match the ventricular outline more accurately to the template than affine only registration. This may explain why the differences between the masked and affine mean images (Fig. 4) are less marked than those for the image-template variance maps (Fig. 5). Most of the source images have enlarged ventricles, and these are not being transformed by the affine procedure; therefore the difference from one scan to another (as reflected by the mean image) is less than the difference from the template (as reflected by the template variance image).

We suggest then that the masked nonlinear approach is both theoretically and practically superior to the affine only technique. However, there are two caveats to this conclusion. First, the masking procedure requires some input from the user—so that the technique is more time consuming, and less objective. However, in practice the required time is not great—being in the order of 30 min per scan. The results from the simulated lesions show that there is little difference in performance for masks defined by different observers, at least at the chosen threshold. This suggests that precise delineation of the lesion and/or artefact is not critical, as long as the areas of major signal change are identified. A second caveat is that the masking technique does not work well when the size of the lesion is large relative to the brain volume. In this situation the nonlinear components have a relatively small area of brain for which the fit is being optimized. The calculated transformations may result in an excellent match within the included area, but allow bizarre transformations in the masked area, where the match is much less constrained. In particular, if a lesion is unilateral, then the match within the masked region is strongly influenced by the data from the homologous region on the opposite side. If the lesion is bilateral, and large, then the transformations within the masked area may be poorly constrained by the data remaining. However, we have found the technique to be robust for unilateral lesions, even for lesions approaching the size of a whole hemisphere (see the second panel from the right in the top row of Fig. 2). Where lesions are large, and nonlinear transformations are used, it may be necessary to increase the weighting for smooth nonlinear deformations (the "nonlinear regularization" in SPM99). This will also reduce the extent to which the nonlinear transformations can match the template and will therefore more closely resemble an affine-only match. In cases where a nonlinear match proves difficult to achieve, an affine-only match may be necessary. In order to avoid bias such as that shown in Fig. 1A we suggest that affine-only normalizations also use a source mask to remove the effect of the lesion.

Normalization using cost function masking may go some way to reducing the problems of interpretation that arise for functional imaging data from patients that have been averaged across subjects. Detecting average activation across subjects is dependent on successful spatial registration of homologous brain areas. If scans from patients have been normalized less successfully than scans for controls, or for other patient groups, then average activation may be reduced or mislocated. Cost function masking appears to offer superior registration to the approaches used thus far and should reduce this problem. However, even for cost function masking, normalizations are likely to be less

successful than those for a normal brain. For a masked brain, a proportion of brain is not available to optimize an accurate match—as shown by the nonzero RMS values for the brains with simulated lesions. Brains from patients may have other more subtle abnormalities outside the masked area, such as enlarged ventricles and sulci. For these reasons, it may still be problematic to compare activation from an averaged group of normal brains to that from an average of lesioned brains. One partial solution might be to pair lesioned and control brains within a study, and use the normalized image of the lesion for the patient to create a matching masking image to use on the unlesioned brain for the control. In this way the quality of the normalizations may be better matched between the patient and control groups.

Methods for normalization with cost function masking are implemented in current software. For example, there are tools for the creation of lesion definition images in AnalyzeAVW (commercial software, Mayo Biomedical Imaging Resource, Mayo Clinic), and MRIcro (free software—http://www.psychology.nottingham.ac.uk/staff/cr1/mricro.html). MRIcro will also create processed source masking images for the normalization [Eq. (4)], and there is a Matlab routine with the same function available at ftp://ftp.mrc-cbu.cam.ac.uk/pub/imaging/Normutils. The standard distribution of SPM99 supports the use of source masking images in normalization, when "object masking" is enabled in the Spatial Normalization section of the program defaults. There is a step by step tutorial on creating and using cost function masking images in normalization with SPM at http://www.psychology.nottingham.ac.uk/staff/cr1/mritut.html. Normalization masking is also a command line option in AIR3 (http://bishopw.loni.ucla.edu/AIR3/).

CONCLUSION

In this paper we have presented and evaluated a technique for spatial normalization of brains with lesions or artefacts. The technique involves masking the abnormal area to prevent the lesion contributing to the normalization. This has the significant theoretical advantage of removing bias in the normalization. Our results suggest that cost function masking provides better and more reliable matching to a standard template than the most-used alternative, which is affine only normalization. We propose that cost-function masking should be used routinely in normalizing brains with areas of abnormal signal; however, comparisons of group activation data for patients with brain lesions with data from controls must still be treated with caution.

ACKNOWLEDGMENTS

M.B. was supported by a grant from the British Brain and Spine Foundation. Many thanks to Dr. Facundo Manes for his kind help in lesion definition.

REFERENCES

Ashburner, J., and Friston, K. J. 1999. Nonlinear spatial normalization using basis functions. *Hum. Brain Mapp.* **7**(4): 254–266.

Ashburner, J., Neelin, P., Collins, D. L., Evans, A. C., and Friston, K. J. 1997. Incorporating prior knowledge into image registration. *NeuroImage* **6:** 344–352.

Ashburner, J., Hutton, C., Frackowiak, R. S. J., Johnsrude, I., Price, C., and Friston, K. J. 1998. Identifying global anatomical differences: Deformation-based morphometry. *NeuroImage* **6:** 348–357.

Collins, D. L., Neelin, P., Peters, T. M., and Evans, A. C. 1994. Automatic 3D intersubject registration of MR volumetric data in standardized Talairach space. *J. Comput. Assist. Tomogr.* **18:** 192–205.

Damasio, A., and Damasio, H. 1989. *Lesion Analysis in Neuropsychology.* Oxford Univ. Press, New York.

Evans, A. C., Dai, W., Collins, D. L., Neelin, P., and Marrett, S. 1991. Warping of a computerized 3-D atlas to match brain image volumes for quantitative neuranatomical and functional analysis. In *Proceedings of the International Society of Optical Engineering: Medical Imaging V,* Vol. 1445, pp. 236–246. SPIE.

Fiez, J. A., Damasio, H., and Grabowski, T. J. 2000. Lesion segmentation and manual warping to reference brain: Intra- and interobserver reliability. *Hum. Brain Mapp.* **9:** 192–211.

Frank, R. J., Damasio, H., and Grabowski, T. J. 1997. Brainvox: An interactive multimodal visualization and analysis system for neuroanatomical imaging. *NeuroImage* **5:** 13–30.

Friston, K. J., Ashburner, J., Frith, C. D., Poline, J.-B., Heather, J. D., and Frackowiak, R. S. J. 1995. Spatial registration and normalization of images. *Human Brain Mapp.* **2:** 165–189.

Hajnal, J. V., Mayers, R., Oatridge, A., Schwieso, J. E., Young, J. R., and Bydder, G. M. 1994. Artifacts due to stimulus correlated motion in functional imaging of the brain. *Magn. Reson. Med.* **31:** 289–291.

Mazzocchi, F., and Vignolo, L. A. 1978. Computer assisted tomography in neuropsychological research: A simple procedure for lesion mapping. *Cortex* **14:** 136–144.

Mummery, C. J., Ashburner, J., Scott, S. K., and Wise, R. J. S. 1999. Functional neuroimaging of speech perception in six normal and two aphasic subjects. *J. Acoust. Soc. Am.* **106:** 449–457.

Musso, M., Weiller, C., Keibel, S., Müller, S. P., Bülau, P., and Rijntjes, M. 1999. Training-induced brain plasticity in aphasia. *Brain* **122:** 1781–1790.

Press, W. H., Teukolsky, S. A., Vetterling, W. T., and Flannery, B. P. 1992. *Numerical Recipes in C,* 2nd ed. Cambridge Univ. Press, Cambridge.

Price, C. J., Howard, D., Patterson, K., Warburton, E. A., Friston, F. J., and Frackowiak, R. S. J. 1998. A functional neuroimaging description of two deep dyslexic patients. *J. Cogn. Neurosci.* **10:** 303–315.

Specht, K., Holtel, C., Weis, S., Herzog, H., Schmidt, D., Mottaghy, F. M., Tellmann, L., Krause, B. J., and Huber, W. 1999. The functional anatomy of auditory lexical decision and its plasticity after left hemisphere damage. *NeuroImage* **9:** S719.

Talairach, J., and Tournoux. 1988. *Coplanar Stereotaxic Atlas of the Human Brain*. Thieme Medical, New York.

Warburton, E., Price, C. J., Swinburn, K., and Wise, R. J. S. 1999. Mechanisms of recovery from aphasia: Evidence from positron emission tomography studies. *J. Neurol. Neurosurg. Psychiatry* **66:** 155–161.

Weiller, C., Isensee, C., Rijntjes, M., Huber, W., Müller, S., Bier, D., Dutschka, K., Woods, R. P., Noth, J., and Diener, H. C. 1995. Recovery from Wernicke's aphasia: A positron emission tomography study. *Ann. Neurol.* **37:** 723–732.

West, J., Fitzpatrick, J. M., Wang, M. Y., Dawant, B. M., Maurer, C. R., Kessler, R. M., Maciunas, R. J., Barillot, C., Lemoine, D., Collignon, A., Maes, F., Suetens, P., Vandermeulen, D., van den Elsen, P. A., Napel, S., Sumanaweera, T. S., Harkness, B., Hemler, P. F., Hill, D. L. G., Hawkes, D. J., Studholme, C., Maintz, J. B. A., Viergever, M. A., Malandain, G., Pennec, X., Noz, M. E., Maguire, G. Q., Pollack, M., Pelizzari, C. A., Robb, R. A., Hanson, D., and Woods, R. P. 1997. Comparison and evaluation of retrospective intermodality brain image registration techniques. *J. Comput. Assist. Tomogr.* **21:** 554–566.

Woods, R. P., Cherry, S. R., and Mazziotta, J. C. 1992. Rapid automated algorithm for aligning and reslicing PET images. *J. Comput. Assist. Tomogr.* **16:** 620–633.